

Toward Feedback Control of Wall Turbulence for Skin Friction Reduction

Nobuhide Kasagi, Koji Fukagata, and Yuji Suzuki
Department of Mechanical Engineering, The University of Tokyo, Japan
Bunkyo-ku, Tokyo 113-8656, Japan

Summary

During the last five years, we have made an extensive research and development study on active feedback control of wall turbulence during the course of the Project for Organized Research Combination System by the Ministry of Education, Culture, Sports and Technology of Japan (MEXT). The present paper introduces some major scientific and engineering accomplishments in our group. Especially, the focus is laid upon the development of hardware system for drag reduction experiment, the relationship between turbulence structure and drag reduction effects, and consideration on the control strategy at high Reynolds number flows.

1 Introduction

The modern turbulence research has a history of more than hundred years since the Osborne Reynolds' pioneering work in the late 19th century. Its three major aims have been to understand highly nonlinear turbulence mechanics, develop predictive methods for turbulent flow phenomena and devise schemes of controlling them. It was this third target that we focused upon, and our efforts have been directed toward innovating highly advanced control methodologies. It is well known that control of turbulent flows and associated transport phenomena should be a key in many engineering practices such as energy saving, efficient production process, securing high quality products, and resolving global environmental problems. Its impacts on future technology and human life would be enormous through manipulation and modification of turbulent drag, noise, heat transfer, mixing as well as chemical reaction.

A collaborative research project on "Smart Control of Turbulence: A Millennium Challenge for Innovative Thermal and Fluids Systems" was started in the fiscal year of 2000, being supported through the Organized Research Combination System by the Ministry of Education, Culture, Sports, Science and Technology (MEXT) (Kasagi et al., 2005). Three national laboratories and several universities participated. In the project, two major control target areas, namely, turbulent wall shear flow and combustion, were identified. For the former target, the authors have mainly worked on the development and application of sensors and actuators fabricated by microelectromechanical systems (MEMS) technology. The final goals are to experimentally achieve friction drag reduction in wall turbulence and to obtain clues toward the use of such an active feedback control system in real applications such as high-speed transportations. In the present paper, the progress in both hardware and software elements are reported.

The paper is organized as follows. In the next section, we overview the development of an active feedback control system for skin friction reduction and its experimental assessment in a wind tunnel. Subsequently, direct numerical simulation (DNS) of turbulent channel flow at moderate Reynolds numbers is introduced, and spatio-temporal characteristics of the near-wall and large-scale vortices are presented for discussions of effective feedback control scheme at higher Reynolds numbers. We then introduce an identity equation, which quantitatively relates the turbulence contribution to the friction drag, and its implication for drag reduction control. We also introduce a theoretical analysis concerning the Reynolds number effect on control by assuming some virtual near-wall layer manipulation.

2 Feedback Control System of Wall Turbulence

The skin friction drag in a wall-bounded turbulent flow is usually much higher than that of a laminar flow at the same Reynolds number. Owing to extensive research over the last several decades, we presently have a common understanding that the large frictional drag in turbulent flows is attributed to the existence of near-wall vortical structure and the associated ejection/sweep events (Kline et al., 1967; Robinson, 1991).

As an example, the spatial relationship between the near-wall quasi-streamwise vortex and the production, destruction and diffusion of the instantaneous Reynolds shear stress is shown in Fig. 1 (Kasagi et al., 1995). A low-pressure region corresponds to the core of an inclined streamwise vortex near the wall. On the sweep side of the vortex, the high-pressure region near the wall is produced by the fluid impingement onto the wall that is induced by the vortex motion. On the ejection side of the vortex, low-speed fluid is lifted up, and its collision against high-speed fluid from upstream forms a local stagnation region with high pressure. Instantaneous high production rate of the Reynolds shear stress takes place on both sides of the vortex. The low- and high-pressure regions are regarded as high destruction (pressure-strain correlation) regions of the Reynolds stress. The turbulent diffusion transports the Reynolds shear stress from the high production regions to the regions between the high- and low-pressure regions.

As described above, the essential dynamical mechanism of near-wall turbulence appears spatially and temporally intermittent. Thus, the production of the turbulent kinetic energy and the wall skin friction could be effectively reduced through selective manipulation of near-wall vortices. Figure 2 shows the spatio-temporal scales of the streamwise vortices in various applications (Kasagi et al., 2003). The typical length scale of vortices is found to be $10\ \mu\text{m}$ to $0.1\ \text{mm}$. Although the coherent structures have such small scales, recent development of MEMS technology has made it possible to fabricate flow sensors and mechanical actuators of such small-scale range (Ho and Tai, 1996).

The aim of our work is to develop an integrated active feedback control system for drag reduction, which is called as “Smart Skin.” To do this, the following research efforts have been made:

- (1) Studies on turbulence physics through a series of direct numerical simulation, and R&D of advanced measurement techniques such as particle image velocimetry.
- (2) Development of sensors and actuators with the aid of MEMS technology and modern electronics.
- (3) Development of turbulence control schemes based on the optimal/suboptimal control theory and adaptive algorithms.

These pieces of work were integrated to develop a prototype turbulence control system. For example, Fig. 3 shows the second-generation control system (Yoshino et al., 2003a). It has four rows of micro hot-film sensors and three rows of miniature magnetic actuators in between. Each sensor row has 48 micro wall-shear stress sensors with $1\ \text{mm}$ spacing, and each actuator row has 16 shell-deformation actuators with $3\ \text{mm}$ spacing. The frequency

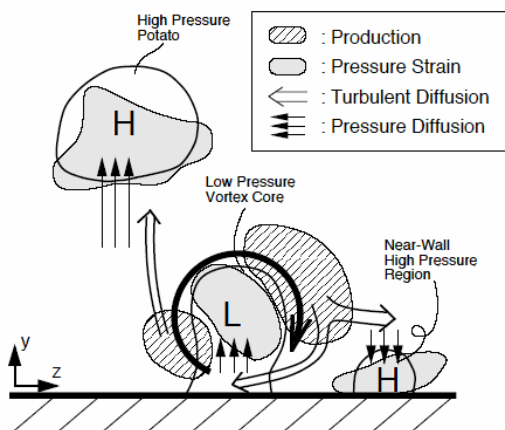


Figure 1 Relationship between a near-wall quasi-streamwise vortex and the production, pressure-strain, and diffusion of $-u'v'$ (Kasagi et al., 1995).

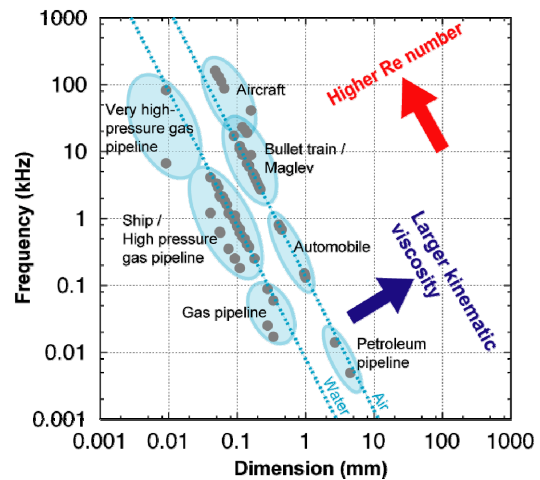


Figure 2 Spatio-temporal scales of coherent structure in real applications (Kasagi et al., 2003).

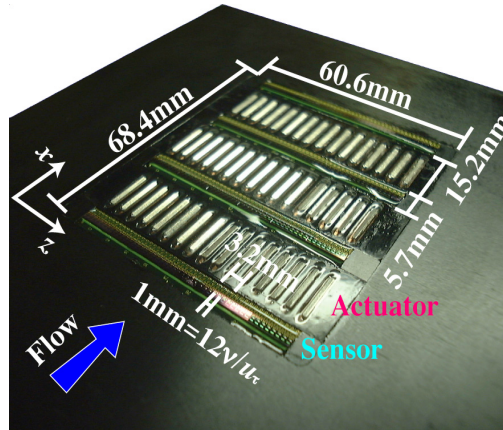


Figure 3 Feedback control system (2nd generation) for wall turbulence with 192 wall shear stress sensors and 48 wall-deformation actuators (Yoshino et al., 2003b).

response of this initial sensor was relatively low, and its gain deteriorated at $f > 270$ Hz (Yoshino et al., 2003b), so that some improvement in its design should be needed. However, it is also found that the spanwise two-point correlation of the wall shear stress measured with the arrayed sensors was in good accordance with the DNS data by Iwamoto et al. (2002). The resonant frequency of the actuator is 800 Hz with the maximum amplitude of about 50 μm . The size and frequency response of these sensors and actuators are found to fulfill the spatio-temporal requirements in the wind tunnel experiment, of which results are described later in this section.

2.1 Control Algorithms for Experimental System

Various control algorithms have been proposed with the aid of direct numerical simulation (Moin and Bewley, 1994; Gad-el-Hak, 1996; Kasagi, 1998; Bewley, 2000; Kim, 2003). Those rigorously based on the modern control theory, e.g., the optimal control theory, are potentially very effective (Bewley et al., 2001). However, much simpler control algorithms are preferable for practical use, as is the case in our experiment, because the amount of measurable flow information is limited and real-time data processing is essential. The above-mentioned knowledge on the near-wall coherent turbulence structures resulted in, for instance, dynamical argument-based control algorithms for drag reduction in turbulent wall-bounded flows.

Choi et al. (1994) demonstrated in their DNS that about 25 % drag reduction can be attained by a simple algorithm, in which local blowing/suction is applied at the wall so as to oppose the wall-normal velocity at 10 wall units above the wall (V-control). Subsequently, several attempts were made to develop control laws using the

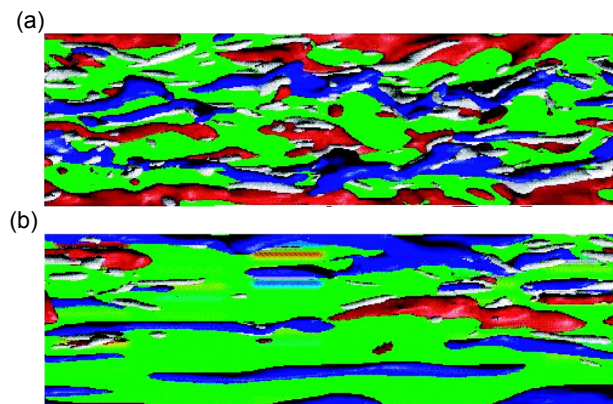


Figure 4 Modification of near-wall turbulence structures (Endo et al., 2000). Blue, low-speed region; red, high-speed region; white, vortex. (a) Uncontrolled; (b) controlled.

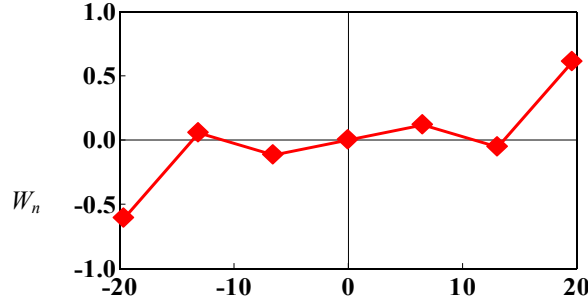


Figure 5 Spanwise distribution of the weights optimized by GA (Morimoto et al., 2002).

quantities measurable at the wall. Lee et al. (1997) used a neural network and found a control law in which the control input is given as a weighted sum of the spanwise wall-shear stresses measured around the actuator. Several analytical solutions of control input to minimize the defined cost function were derived by Lee et al. (1998) in the framework of the suboptimal control. Their DNS of channel flow at $Re_\tau = 110$ showed 16-22% drag reduction by using the spanwise wall shear stress or the wall pressure as a sensor signal; in the former case, the control law is quite similar to that obtained by using the neural network mentioned above. Koumoutsakos (1999) presented a scheme to control the vorticity flux and succeeded in reducing the friction drag in DNS, where the wall pressure was used as a sensed flow signal.

There are two major difficulties in the above-mentioned control schemes to be implemented in real turbulence control system. First, the control input assumed in the previous studies was blowing/suction, which distributed continuously over the wall surface. However, it is unknown how much the control effectiveness would be deteriorated if discrete sensors and actuators of certain sizes are distributed on the wall. Moreover, instead of blowing/suction, wall-deformation actuators are more plausible for practical design. Endo et al. (2000) carried out DNS of a turbulent channel flow, in which arrayed wall shear stress sensors and wall-deformation actuators were implemented. Instantaneous streamwise and spanwise wall shear stresses were measured, so that the wall deformation actuators were triggered so as to attenuate the meandering motion of low-speed streaks. In their DNS of channel flow at $Re_\tau = 110$, the low-speed streaks were stabilized as shown in Fig. 4, and the substantial drag reduction of 12% was attained.

Another issue is that various flow quantities assumed to be monitored for state feedback in DNS studies are very difficult to measure in reality. The only exception would be streamwise wall shear stress or wall pressure. To resolve this, a methodology based on the genetic algorithm (GA) has been developed by Morimoto et al. (2002). The control input (i.e., blowing/suction velocity), v_w , was assumed to be a weighted sum of streamwise wall shear stresses, τ_w , around an actuator, i.e.,

$$v_w(x, z, t) = C \left(\sum_n W_n \tau_w(x, z + n\Delta z, t) \right), \quad (1)$$

where C is the amplitude factor. The weights, W_n , were optimized through the genetic operation, i.e., the selection, mutation, and crossover, so as to minimize the friction drag.

About 6000 runs of DNS of channel flow at $Re_\tau = 110$ were repeated for optimizing weights. As a result, about 12% drag reduction was achieved by employing a set of the optimized weights, which are shown in Fig. 5. Generally speaking, the correlation between the streamwise wall shear stress τ_w and the wall-normal velocity induced by the near-wall vortices is small, which makes it difficult to mimic V-control (Choi et al., 1994) using τ_w . However, the wall blowing/suction with the asymmetric weights shown in Fig. 5 makes the velocity distribution at the bottom of streaky structures shifted and tilted in the spanwise direction. Therefore, the wall-normal velocity is in-phase with τ_w , and the present control becomes similar to V-control. This result suggests possible employment of τ_w as sensor information for feedback control. It is also theoretically found that this distribution of weights selectively enhances spanwise wave components of 80 wall units.

2.2 Control Experiments

Performance evaluation of the feedback control system shown in Fig. 3 is made in a turbulent channel air flow. The cross section of the channel is $50 \text{ mm} \times 500 \text{ mm}$, and the test section is located 4 m downstream from the inlet, where the flow is fully developed. The control system is placed at the bottom wall of the test section. The bulk mean velocity is set to be 3 m/s, which corresponds to the friction Reynolds number of 300. Under the present flow condition, one viscous length and time units correspond to 0.09 mm and 0.5 ms, respectively. Thus, the mean diameter of the near-wall streamwise vortices is estimated to be 2.7 mm (or 30 length units), while its characteristic time scale is 7.5 ms (or 15 time units). The flow is measured with a three-beam two-component LDV system (DANTEC, 60X51). The measurement volume is about $\phi 160 \mu\text{m} \times 3.5 \text{ mm}$.

An optimal control scheme based on genetic algorithm (GA) mentioned above (Morimoto et al., 2002) is employed in the present experiment. Driving voltage of each wall-deformation actuator, E_A , is determined with a linear combination of the streamwise wall shear stress fluctuations, $\tau'_{w,i}$, i.e.,

$$E_A = \sum_{i=1}^3 W_i \tau'_{w,i}, \quad (2)$$

where $\tau'_{w,i}$ is measured by three sensors located upstream of the actuator. The spacing between neighboring sensors used in the present control scheme is 36 viscous units. Note that actuators move upwards when E_A is positive, while downwards when negative. The weights, W_i , are optimized in such a way that the mean wall shear stress measured by three sensors at the most downstream location is minimized. The cost function to be maximized, J , is defined by

$$J = 1 - \frac{\sum_{j=1}^3 \left(\int_0^T \tau_{w,j} dt \right)}{\sum_{j=1}^3 \left(\int_0^T \tau_{w,j}^u dt \right)}, \quad (3)$$

where $\tau_{w,i}^u$ is the wall-shear of the uncontrolled flow. Note that J is identical to the drag reduction rate. Each weight, W_i , is expressed with a binary-coded string of 5 bits. This string corresponds to a gene, and N individuals including a set of genes are made. Feedback control experiment using each individual, i.e., a different set of weights, is independently carried out, and the cost function is calculated online. Then, individuals which give smaller cost are statistically selected as parents, and offsprings are made through crossover operation. Finally, mutation is applied to all genes of N individuals at a prescribed rate. The elite selection strategy is also adopted, so that the gene that has the maximum cost is preserved. New generations are successively produced by repeating this procedure. The integration time T is chosen as 20 s ($T^+ = 4000$).

Figure 6(a) shows the evolution of the cost function (Suzuki et al., 2005). The data are scattered in a wide range because of the genes with random number introduced, but the degree of drag reduction is estimated to be $6 \pm 3\%$ by accounting for 3% measurement uncertainty in J . Figure 6(b) shows the distribution of optimum weights, which

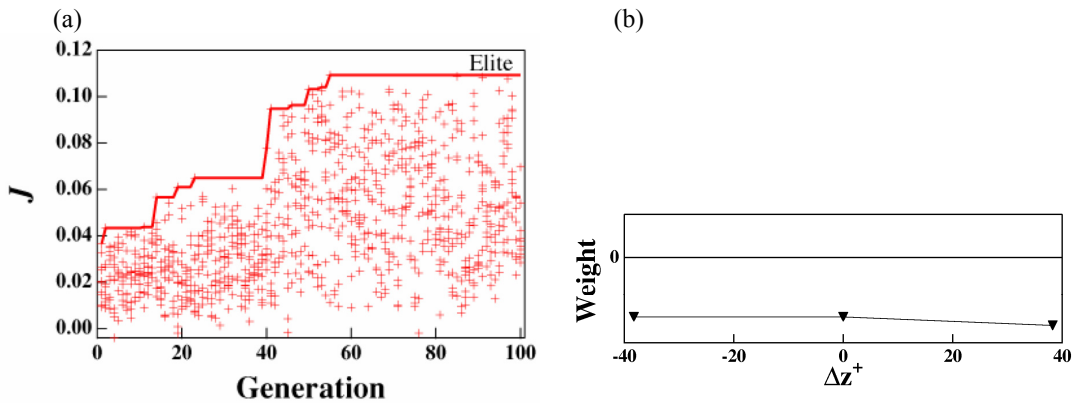


Figure 6 Result of GA-based feedback control in a turbulent channel flow. (a) Cost function versus generation; (b) Optimum weight distribution (Suzuki et al., 2005).

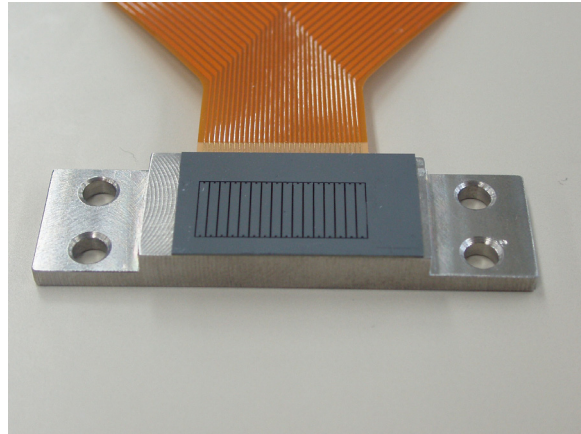


Figure 7 MEMS-fabricated seesaw type magnetic actuator array. One actuator size is $1\text{mm} \times 7\text{mm}$ (Yamagami et al., 2005).

corresponds to the optimum gene obtained. It is found that all weights are negative, and about half of the genes tested in the present experiment have a similar trend. Therefore, drag reduction is achieved with negative weights in the present experiment. Note that, when all weights are kept positive without using the GA algorithm, no drag reduction is obtained (not shown here).

A prototype of fully MEMS-based integrated control system is also under development (Yamagami et al., 2005). It consists of micro hot-film shear stress sensors with backside electronic contact, MEMS-fabricated seesaw type magnetic actuators of low energy consumption as shown in Fig. 7, and a custom-made analog VLSI controller. The assessment of this system remains to be a future study.

3 Toward Control at High Reynolds Numbers

Up to now, various Reynolds number effects in wall turbulence have been reported. Zagarola and Smits (1998) suggest that the overlap region between inner and outer scalings in wall-bounded turbulence may yield a log law rather than a power law at very high Reynolds numbers. Moser et al. (1999) have made DNS of fully-developed turbulent channel flows at $Re_\tau = 180\text{-}590$, and they conclude that the wall-limiting behavior of rms velocity fluctuations strongly depends on the Reynolds number, but obvious low-Reynolds-number effects are absent at $Re_\tau = 395$. It is well known that near-wall streamwise vortices play an important role in the transport mechanism in wall turbulence, at least, at low Reynolds number flows (Robinson, 1991; Kravchenko et al., 1993; Kasagi et al., 1995). Those streamwise vortices and streaky structures, which are scaled with the viscous wall units (Kline et al., 1967), are closely associated with the regeneration mechanism (Hamilton et al., 1995).

On the other hand, the relationship between the near-wall coherent structures and the large-scale outer-layer structures at higher Reynolds numbers still has not been fully resolved. Adrian et al. (2000) show that packets of

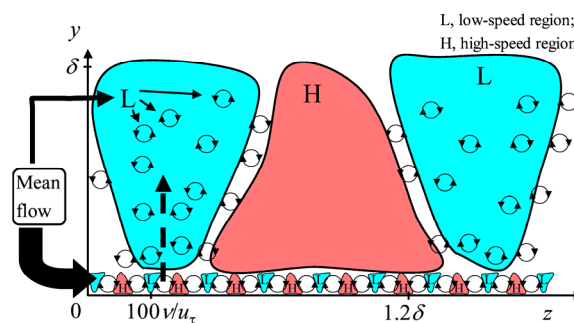


Figure 8 Conceptual diagram of energy flow between the near-wall vortices and the large-scale outer-layer structures (Iwamoto et al., 2004).

large-scale hairpin vortices around the low-speed large-scale structures are often observed in high-Reynolds-number wall turbulence. Zhou et al. (1999) have studied the evolution of a single hairpin vortex-like structure in a low-Reynolds-number channel flow through DNS, and found a packet of hairpins that propagate coherently as reported in Adrian et al. (2000).

Figure 8 shows a conceptual diagram of the turbulent kinetic energy paths between the near-wall vortices and the large-scale outer-layer structures. The near-wall vortices extract a large amount of turbulent kinetic energy from the mean flow. Most energy dissipates by themselves, while the rest is transferred to the large-scale structures through the nonlinear interaction (Iwamoto et al., 2002). On the other hand, the large-scale structures also gain substantial energy from the mean flow. The energy is not dissipated by themselves, but transferred to the smaller vortices through the energy cascade. The following contradictory hypotheses about the origin of the large-scale structures are considered:

- (1) The near-wall streamwise vortices agglomerate autonomously, and form clustered structures, which result in the low-speed large-scale outer-layer structures. Therefore, the energy transfer from the near-wall coherent structures to the large-scale structures is directly associated with formation of the latter structures.
- (2) The large-scale structures exist independently due to their own self-sustaining mechanism. The near-wall small-scale vortices do not agglomerate autonomously, but they are clustered by the advective motion of the low-speed large-scale structures. Therefore, the direct energy transfer from the mean flow to the large-scale structures is indispensable for producing the large-scale structures.

In order to examine the above-mentioned hypotheses, DNSs of turbulent channel flow at moderately high Reynolds numbers of $Re_\tau = 650$ and 1160 have been carried out (Iwamoto et al., 2004), and an overview of the results is given below.

3.1 Large-Scale Structures

The fundamental characteristics of the near-wall coherent structures and large-scale structures are evaluated through DNS. The numerical method used in the present study is almost the same as that of Kim et al. (1987); a pseudo-spectral method with Fourier series is employed in the streamwise (x) and spanwise (z) directions, while a Chebyshev polynomial expansion is used in the wall-normal (y) direction. A fourth-order Runge-Kutta scheme and a second-order Crank-Nicolson scheme are used for time discretization of the nonlinear and viscous terms, respectively. The average of pressure gradient is kept constant.

For $Re_\tau = 1160$, the size of the computational domain is $6\pi\delta \times 2\delta \times 2\pi\delta$, and the wave number is $1152 \times 513 \times 1024$ in the x -, y -, and z -directions, respectively. The 3/2 rule is applied in order to avoid aliasing errors arising in computing the nonlinear terms pseudo-spectrally. The number of the total grid points is about 2 billions, and the effective computational speed is about 1.4 TFLOPS by using 512 CPUs and 600 GB main memory on the Earth Simulator. The two-point correlations in the x - and z -directions at any y -locations fall off to zero values for large separations, indicating that the computational domain is sufficiently large. The energy density associated with high wave numbers is by several orders of magnitude lower than the energy density corresponding to low wave numbers, and this means the grid resolution is sufficiently fine. Hereafter, u , v , and w denote the velocity components in the x -,

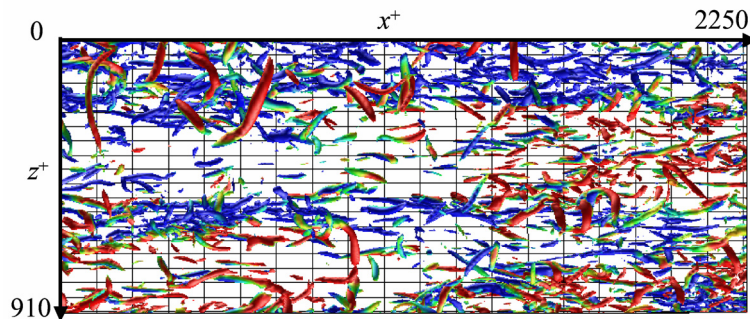


Figure 9 Top view of vortices at $Re_\tau = 1160$ (Iwamoto et al., 2004). Iso-surface, $Q^+ = -0.02$; blue to red, $u^{+} = -1$ to $u^{+} = 1$. Total computational volume is 21865 and 7288 wall units in the x - and z -directions, respectively.

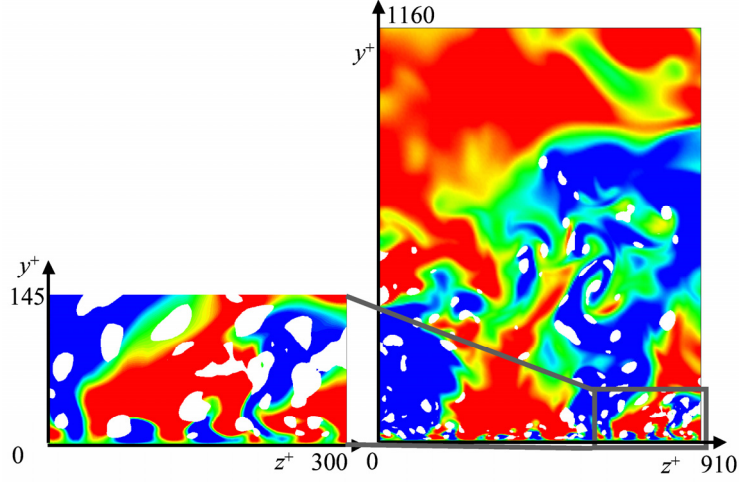


Figure 10 Cross-stream sectional view of instantaneous velocity field at $Re_\tau = 1160$ (Iwamoto et al., 2004). Contours of streamwise velocity fluctuation, blue to red, $u^+ = -1$ to $u^+ = 1$; white, $Q^+ < 0.005$. Total computational volume is 2320 and 7288 wall units in the y - z directions, respectively.

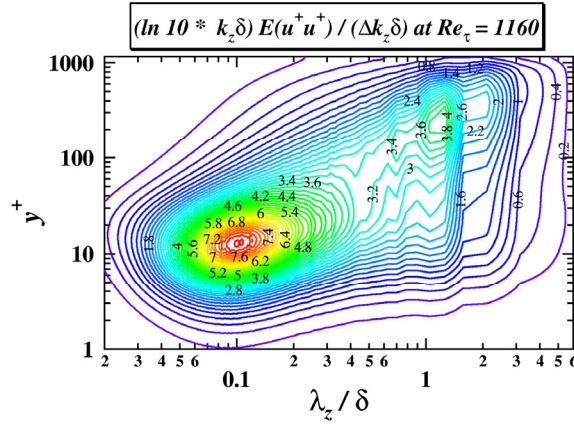


Figure 11 Contour of one-dimensional spanwise pre-multiplied power spectra of u' at $Re_\tau = 1160$ (Iwamoto et al., 2004).

y -, and z -directions, respectively. Superscript (+) represents quantities non-dimensionalized with u_τ and ν .

The vortices identified with iso-surfaces of the second invariant of the deformation tensor ($Q^+ = 0.02$) are visualized in an x - z plane of an instantaneous flow field at $Re_\tau = 1160$ as shown in Fig. 9. It is found that the vortices form clusters in low-speed regions, and that some hairpin vortices are observed in high-speed regions.

Figure 10 shows contours of the streamwise velocity fluctuation u and vortices ($Q^+ \leq 0.005$) in a y - z cross-stream plane in order to examine the relationship between the near-wall vortices and the large-scale outer-layer structures. The near-wall vortices are located between low- and high-speed streaky structures as same as those in low Reynolds number flows (Kasagi et al., 1995). Away from the wall, large-scale low/high-speed regions exist, and small-scale vortices are found mostly in the low-speed region. The streaky structures, of which spanwise spacing is about 100 wall units, exist only near the wall ($y^+ \leq 30$), while the large-scale structures extend from the channel center to the near-wall region ($y^+ \leq 30$).

Figure 11 shows the one-dimensional spanwise pre-multiplied power spectra of u . The obvious peak exists at $y^+ \approx 15$ and spanwise wavelength $\lambda_z^+ \approx 120$ ($\lambda_z / \delta \approx 0.1$), indicating that the near-wall streaky structures have large contribution to the near-wall streamwise velocity fluctuations as in low-Reynolds-number flows. On the other hand, a weak second peak can be also identified at $y^+ \approx 300$ and $\lambda_z / \delta \approx 1.2$, which is only observed in this higher Reynolds number.

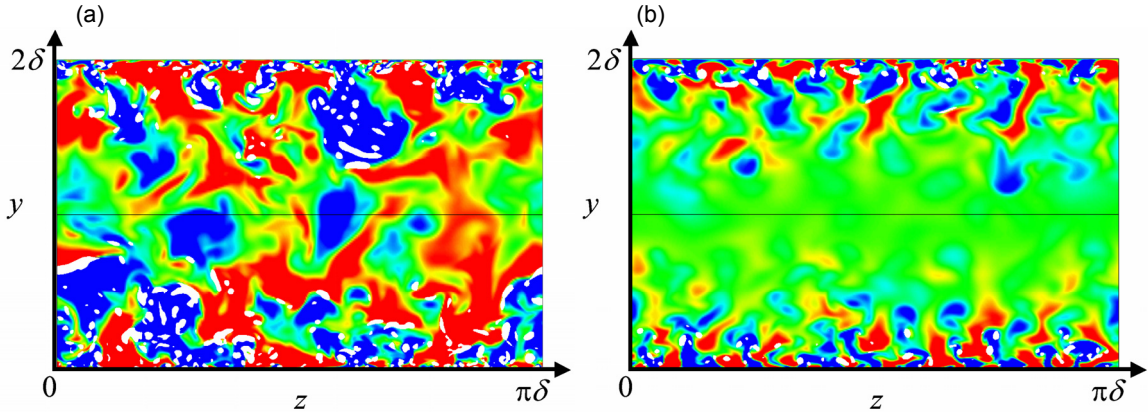


Figure 12 Cross-stream sectional view of instantaneous velocity field at $Re_\tau = 650$ (Iwamoto et al., 2004). (a) Original flow; (b) with intercept of the energy transfer from the mean flow to the large-scale structures. Contours as in Fig. 10.

3.2 Origin of Large-Scale Structures

The origin of the large-scale structures is studied through DNS at $Re_\tau = 650$. The computational method is the same as that of $Re_\tau = 1160$. In order to examine the effect of the energy production in the large-scale structures, the energy transfer from the mean flow to the large-scale structures is intercepted by using the Navier-Stokes equation with an additional blocking term (Iwamoto et al., 2004). Since the large-scale structures have the streamwise normal Reynolds stress mainly in the range of $\lambda_z/\delta > 0.6$ as shown in Fig. 11, the blocking is applied only for the spanwise wavelength $\lambda_z/\delta > 0.6$. A fully developed flow field is used as the initial condition, and the mean velocity profile is fixed in order to hold the Reynolds number.

Figure 12 shows contours of the instantaneous streamwise velocity fluctuation u' and the vortices in a cross-stream plane. The large-scale structures exist from the center of the channel to the near-wall region in the original turbulent channel flow, and the smaller vortices are clustered in the low-speed large-scale structures. On the other hand, when the energy transfer is intercepted, the large-scale structures and the clustered vortices disappear. Therefore, the direct energy transfer from the mean flow to the large-scale structures is indispensable for the generation of the large-scale structures. Moreover, the small-scale vortices do not agglomerate autonomously, and they are not clustered without the motion of the low-speed large-scale structure.

4 The FIK Identity

Despite the extensive research on wall-turbulence, the quantitative relation between the statistical quantities of turbulence and the drag reduction effect has not been completely clear. Recently, we derived a mathematical relation between the skin friction coefficient and the Reynolds stress distribution for three canonical wall-bounded flows, i.e., channel, pipe and plane boundary layer flows (Fukagata et al., 2002) (hereafter, referred to as the FIK identity). Although the derivation itself is simple and straightforward, the result is suggestive and useful for analyzing the effect of the Reynolds stress on the frictional drag, especially for controlled flows.

The overview of the derivation process is as follows. For a fully developed channel flow, the Reynolds averaged Navier-Stokes equation in the x direction is given by

$$0 = -\frac{d\bar{p}}{dx} + \frac{d}{dy} \left[\frac{1}{Re_b} \frac{d\bar{u}}{dy} + (-\overline{u'v'}) \right], \quad (4)$$

where the overbar denotes the average. In this section, all variables without superscript are those nondimensionalized by the channel half width δ^* , and twice the bulk mean velocity $2U_b^*$, whereas dimensional variables are denoted by the superscript of $*$. The bulk Reynolds number is defined as $Re_b = 2U_b^* \delta^* / \nu^*$, where ν^* is

the kinematic viscosity. The pressure in Eq. (4) is normalized by the density.

By applying a triple integration to Eq. (4) and integration by parts, we obtain the FIK identity for a fully developed channel flow, i.e.,

$$C_f = \frac{12}{Re_b} + 12 \int_0^1 2(1-y)(-\overline{u'v'}) dy, \quad (5)$$

where $y = 0$ and 1 correspond to the wall and the channel center, respectively. This identity equation indicates that the skin friction coefficient is decomposed into the laminar contribution, $12/Re_b$, which is identical to the well-known laminar solution, and the turbulent contribution (the second term), which is proportional to the weighted average of Reynolds stress. The weight linearly decreases with the distance from the wall.

A similar relationship can be derived also for other canonical flows. The FIK identity for a fully-developed cylindrical pipe flow is

$$C_f = \frac{16}{Re_b} + 16 \int_0^1 2r \overline{u'_r u'_z} r dr. \quad (6)$$

Here, the length is nondimensionalized by the pipe radius. The FIK identity for a zero pressure-gradient boundary layer on a flat plate is

$$C_f = \frac{4(1-\delta_d)}{Re_\delta} + 4 \int_0^1 (1-y)(-\overline{u'v'}) dy - 2 \int_0^1 (1-y)^2 \left(\frac{\partial \overline{uu}}{\partial x} + \frac{\partial \overline{uv}}{\partial y} \right) dy, \quad (7)$$

where the nondimensionization is based on the free-stream velocity and the 99% boundary layer thickness. The third term is the contribution from the spatial development and δ_d in the first term is the dimensionless displacement thickness. For a laminar plane boundary layer, the first contribution is $4(1-\delta_d)/Re_\delta \approx 2.6/Re_\delta$ and the third contribution can be computed as $2.6/Re_\delta$ by using the similar solution of Howarth (1938). The summation of these contributions is identical to the well-known relation, i.e., $C_f \approx 3.3/Re_\delta$.

4.1 General Form of the FIK Identity

A more general form of the FIK identity (e.g., for channel flows) can be expressed as

$$C_f = \frac{12}{Re_b} + 12 \int_0^1 2(1-y)(-\overline{u'v'}) dy + \text{(III)} + \text{(IV)} + \text{(V)}. \quad (8)$$

The third term is the contribution from the spatial and temporal development, which reads

$$\text{(III)} = 12 \int_0^1 (1-y)^2 \left(-\frac{\partial (uu)''}{\partial x} - \frac{\partial (uv)''}{\partial x} + \frac{1}{Re_b} \frac{\partial^2 u''}{\partial x^2} - \frac{\partial p''}{\partial x} - \frac{\partial u''}{\partial t} \right) dy, \quad (9)$$

where the double-prime denotes the deviation of mean quantity from the bulk mean quantity, i.e.,

$$f''(x, y, t) = \overline{f}(x, y, t) - \int_0^1 \overline{f}(x, y, t) dy. \quad (10)$$

The fourth term is the contribution from body force, b_x , and additional stress, τ_{xy}^a , such as that by polymer/surfactant (Yu et al., 2004; Li et al., 2004; Hou et al., 2006), which can be expressed as

$$(IV) = 12 \int_0^1 (1-y) \left[(1-y) \overline{b_x} + 2 \overline{\tau_{xy}^a} \right] dy. \quad (11)$$

The fifth term is the contribution from the boundary momentum flux, such as uniform blowing/suction, i.e.,

$$(V) = -12 V_w \int_0^2 (1-y) \overline{u} dy, \quad (12)$$

where V_w denotes the wall-normal velocity at the walls. In this case, the integration of other terms should also be done from 0 to 2, because the flow is not anymore symmetric around the center plane.

4.2 Analysis of Drag-Reducing Flows

The merit of the relations derived above is that one can quantitatively identify each dynamical contribution to the drag reduction/enhancement even for a manipulated flow, and some examples follow below.

The first example is a fully developed turbulent pipe flow controlled by the opposition control (Choi et al., 1994). The data were obtained by DNS using the energy-conservative finite difference method (Fukagata and Kasagi, 2002) at the Reynolds number of $Re_b = 5300$ (i.e., $Re_\tau = 180$ for uncontrolled flow). The detection plane is set at $y_d^+ = 15$. Here, the superscript of + denotes a quantity nondimensionalized by the friction velocity of the uncontrolled flow.

Figure 13 shows the Reynolds shear stress, $\overline{u_r' u_z'}$, and the weighted Reynolds shear stress appearing in Eq. (6) (i.e., $2r^2 \overline{u_r' u_z'}$). As is noticed in Eq. (6), the contribution of Reynolds stress near the wall dominates both in uncontrolled and controlled cases. The difference in the areas covered by these two (controlled and uncontrolled) curves of the weighted Reynolds stress is directly proportional to the drag reduction by control. In the present case, the turbulent contribution is reduced by 35%, while the total drag reduction is 24% because of the additional laminar contribution. The contribution of Reynolds stress near the wall can be more clearly illustrated by plotting a cumulative contribution, $C_f^{T(cum)}$, to the turbulent part defined here as,

$$C_f^{T(cum)}(y) = 16 \int_0^{1-y} 2r \overline{u_r' u_z'} r dr, \quad (13)$$

where $y = (1-r)$ is the distance from the wall. As is shown in Fig. 14, the Reynolds stress within 80 wall units from the wall is responsible for 90% of the turbulent contribution to the skin friction in the case of uncontrolled flow. This fact makes the opposition control algorithm proposed by Choi et al. (1994) very successful. Namely, it works to suppress the Reynolds stress near the wall, and this results in considerable drag reduction at a low Reynolds number flow.

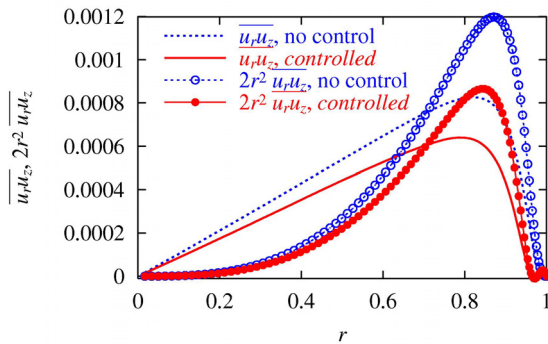


Figure 13 Reynolds shear stress and weighted Reynolds shear stress in pipe flow at $Re_\tau = 180$ under opposition control (Fukagata et al., 2002).

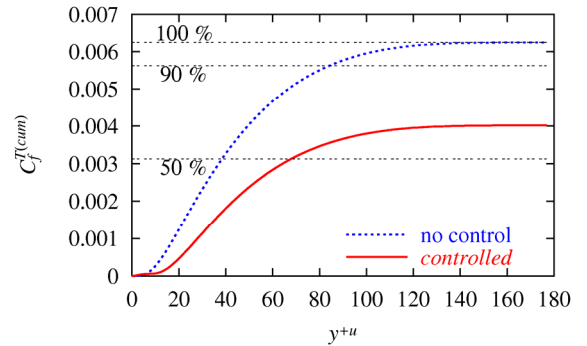


Figure 14 Cumulative contribution of Reynolds stress to skin friction in pipe flow at $Re_\tau = 180$ under opposition control (Fukagata et al., 2002).

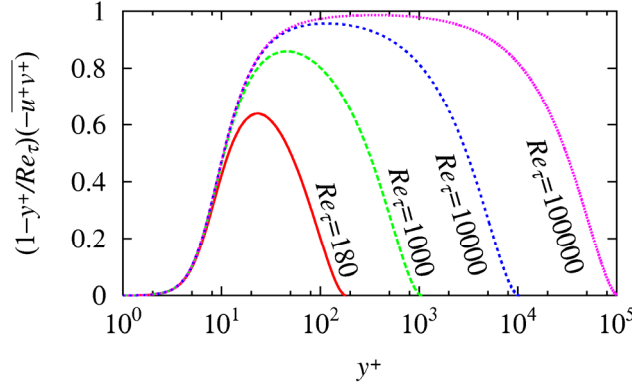


Figure 15 Weighted Reynolds shear stress at different Reynolds numbers (model calculation).

A more interesting analysis can be made when the feedback control is applied only partially to the wall (Fukagata and Kasagi, 2003). By using the FIK identity, one can formulate the budget equation for the spatial transient of friction drag. Thus, the mechanism of drag reduction after the onset of control and that of drag recovery in the downstream uncontrolled region can be quantitatively discussed. The analysis suggested that the direct effect of the opposition control (Choi et al., 1994) is limited to the near-wall region and the changes of flow statistics in the region far from the wall is due to an indirect effect.

Figure 15 shows the profiles of weighted Reynolds shear stress in uncontrolled flow at different Reynolds numbers, which are calculated by using a simple mixing length model. At higher Reynolds numbers, the contribution of near-wall Reynolds shear stress to the friction drag drastically decreases and the contribution of the large-scale structure (discussed in the previous section) becomes dominant. However, as mentioned just above, the Reynolds shear stress far from the wall can also be reduced by near-wall manipulation. Then, the question is whether the near-wall flow manipulation is sufficiently effective to friction drag reduction even in practical applications at high Reynolds numbers. An attempt to answer this question is introduced in the next section.

Another example of analysis is a fully developed channel flow with uniform blowing on one wall and suction on the other. Figure 16 shows the componential contributions computed from the database (Sumitani and Kasagi, 1995), where the blowing/suction velocity is $V_w = V_w^*/(2U_b^*) = 0.00172$. For comparison, the case with $V_w = 0$ (an ordinary channel flow) at the same bulk Reynolds number ($Re_b = 4360$) was also computed by the pseudospectral DNS code (Iwamoto et al., 2002).

The weighted Reynolds shear stress on the blowing side (defined here, for convenience, as $0 \leq y \leq 1$) is larger than that in the case of $V_w = 0$, while it is close to zero on the suction side ($1 \leq y \leq 2$). The total turbulent contribution is slightly reduced from the ordinary channel flow. The convective contribution, i.e., the integrand of

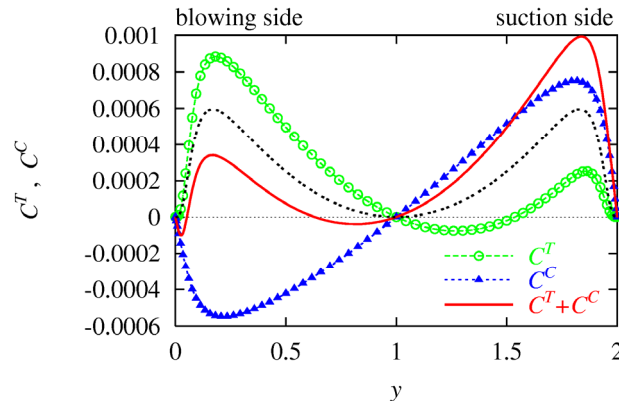


Figure 16 Contributions to friction drag in a channel flow at $Re_\tau = 150$ with uniform blowing/suction (Fukagata et al., 2002). The keys, C^T and C^C , denote the integrand of turbulent and convective contributions, respectively.

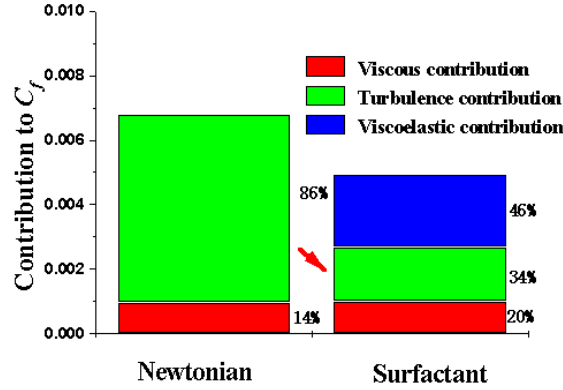


Figure 17 Decomposed contributions to friction drag in a water channel flow with surfactant (Yu et al., 2004).

Eq. (12), is negative on the blowing side and positive on the suction side. The total convective contribution of Eq. (12) is slightly positive. Since the total convective contribution exceeds the amount of reduction in the turbulent contribution, the total C_f results in a larger value than that of the ordinary channel flow.

The last example of analysis is a surfactant-added channel flow (Yu et al., 2004). DNS is performed by assuming the Giesekus fluid model. The bulk Reynolds number is 12000. The friction Weissenberg number, which represents the memory effect of the surfactant-added fluid, is 54, corresponding to 75 ppm CTAC surfactant solution. The fractional contribution to C_f is shown in Fig. 17, where the turbulent contribution drastically decreases with the addition of surfactant. The viscoelastic contribution of Eq. (11), however, works to largely increase the friction drag. As a result of these changes, the total friction drag is reduced by about 30%. A similar analysis for an experimental data of polymer-added boundary layer is also reported (Hou et al., 2006). The changes in the different contributions are qualitatively similar to those of the surfactant-added flow introduced above.

4.3 Development of Control Schemes

The above knowledge suggests that suppression of the Reynolds shear stress in the near-wall region is of primary importance in order to reduce the skin friction drag. Once the near-wall Reynolds shear stress is suppressed, the stress far from the wall is also suppressed through the indirect effect (Fukagata and Kasagi, 2003). From this argument, a new suboptimal control law is derived by Fukagata and Kasagi (2004a). In that work, the cost functional for a channel flow was defined as follows:

$$J(\phi) = \frac{\ell}{2A\Delta t} \int_t^{t+\Delta t} \int_S \phi^2 dS dt + \frac{1}{2A\Delta t} \int_t^{t+\Delta t} \int_S (-u'v')_{y=Y} dS dt. \quad (14)$$

Here, ϕ denotes the control input, i.e., the blowing/suction velocity at the wall, A is the area of wall, Δt is the time-span for optimization, and ℓ is the price for the control.

The Reynolds shear stress above the wall (at $y = Y$) is approximated by using a first-order Taylor expansion to yield an approximated cost functional, i.e.,

$$(-u'v')_{y=Y} = -Y\phi \left. \frac{\partial u}{\partial y} \right|_w \quad (15)$$

The control input, ϕ , that minimizes the cost functional, can be calculated analytically by the procedure proposed by Lee et al. (1998). As the result, the suboptimal control input is obtained as

$$\hat{\phi} = \frac{\alpha}{1 - i\alpha\gamma k_x/k} \left. \frac{\partial \hat{u}}{\partial y} \right|_w, \quad (16)$$

where the hat denotes the Fourier component, $i = \sqrt{-1}$ and $k = \sqrt{k_x^2 + k_z^2}$. There are two parameters in this algorithm: $\alpha = Y/(2\ell)$ is the amplitude coefficient and $\gamma = \sqrt{2Re_b/\Delta t}$ can be interpreted as an inverse of influential length (see, Fukagata and Kasagi (2004), for details).

A similar algorithm can be developed also for a pipe flow. Following the procedure by Xu et al. (2002), we obtain an approximate control law, which reads

$$\hat{\phi} = \frac{\alpha}{1 - i\alpha\gamma I_m(k_z)/I'_m(k_z)} \left. \frac{\partial \hat{u}_z}{\partial r} \right|_w, \quad (17)$$

where I_m is an m th-order modified Bessel function of the first kind and I'_m is its derivative. Although the expressions look different, the control laws for channel and pipe have essentially the same dynamical effect on the controlled flow (Fukagata and Kasagi, 2004a).

The derived control algorithm can be transformed to the physical space through the following inverse Fourier transform, similarly to Lee et al. (1998). The weight distribution in the physical space is shown in Fig. 18. They are symmetric in the spanwise direction and asymmetric in the streamwise direction. The product of parameters, $\alpha\gamma$, determines the tail length in the streamwise direction.

Performance of the proposed control algorithm is tested by DNS of turbulent pipe flow. About 12 % drag reduction is obtained when ϕ_{rms}^+ is around 0.1 and $\alpha\gamma = 73$. The profile of the Reynolds shear stress is shown in Fig. 19. As expected, the near-wall Reynolds stress is suppressed by the present control. As can be seen from the comparison, the profile of the present control is nearly the same as that of the opposition control (denoted as v -control) with $y_d^+ = 5$. Comparison is also made with the opposition control with $y_d^+ = 15$, in which the Reynolds stress around $5 < y^+ < 10$ is suppressed to give a higher drag reduction rate of 25%. The direct suppression with the present control seems to occur merely in the region of $0 < y^+ < 5$. This is due to the first-order Taylor expansion used for the approximation of cost functional, i.e., Eq. (15). If streamwise velocity above the wall, say at $y^+ = 15$, can be more accurately estimated, a higher drag reduction can be made by this control strategy. In fact, in DNS using the streamwise velocity above the wall as an idealized sensor signal, a drag reduction rate comparable to the opposition control (about 25%) was attained (Fukagata and Kasagi, 2004b).

Finally, the FIK identity further suggests that a drastic drag reduction can be achieved if the near-wall Reynolds

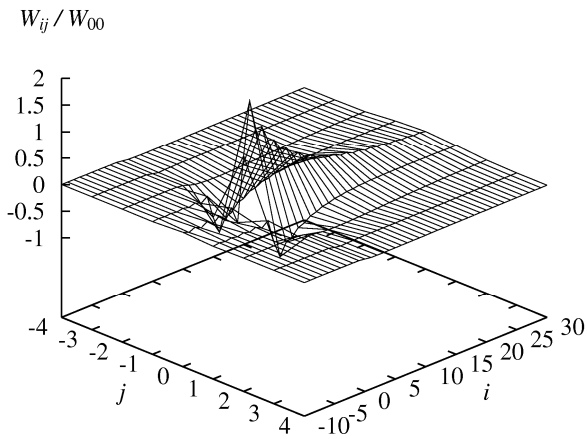


Figure 18 Weight distributions of the Reynolds shear stress-based suboptimal control law (Fukagata and Kasagi, 2004a). Indices i and j denote the streamwise and spanwise grid numbers, respectively, from the blowing/suction point.

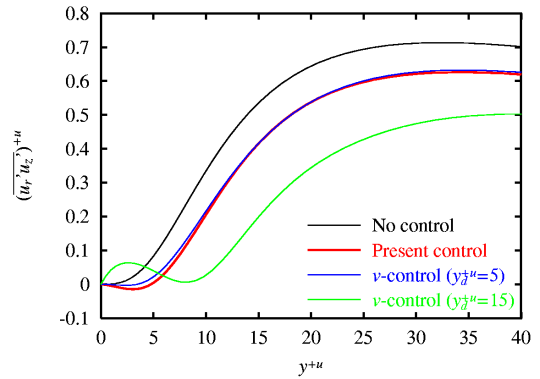


Figure 19 Reynolds shear stress in pipe flow at $Re_\tau = 180$ under the Reynolds shear stress-based suboptimal control (Fukagata and Kasagi, 2004a).

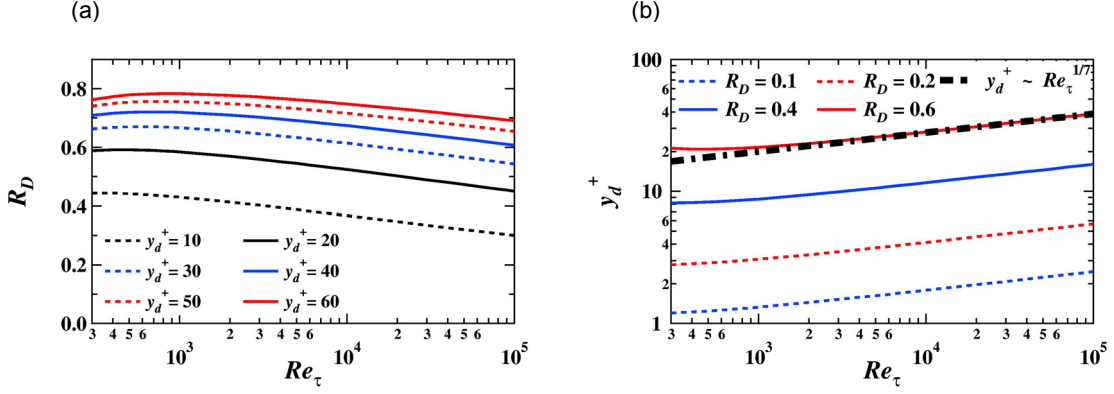


Figure 20 Theoretical Reynolds number dependency of idealized near-wall manipulation (Iwamoto et al., 2005). (a) Dependency of drag reduction rate, R_D , on Reynolds number, Re_τ , with constant thickness damping layer, y_d^+ ; (b) Thickness of damping layer, y_d^+ , required for prescribed drag reduction rate, R_D .

shear stress is more ideally reduced. When an ideal feedback body force (instead of blowing/suction) is applied to DNS, the near-wall Reynolds shear stress became negative to yield a friction drag much lower than that of the laminar flow (Fukagata et al., 2005). In that case, however, the actuating power consumption becomes larger than the power saved by the drag reduction.

5 Control Feasibility at High Reynolds Numbers

The Reynolds number assumed in most previous studies on active feedback control of wall-turbulence remains at $Re_\tau = 100-180$, where significant low-Reynolds-number effects must exist. Iwamoto et al. (2002) showed in their DNS at $Re_\tau < 642$ that the effect of the suboptimal control (Lee et al., 1998) is gradually deteriorated as the Reynolds number is increased. In real applications, the Reynolds number is far beyond the values that DNS can handle. For a Boeing 747 aircraft, for example, the friction Reynolds number is roughly estimated to be $Re_\tau \sim 10^5$ under a typical cruising condition. For such high Reynolds number flows, where highly complex turbulent structures exist with a very wide range of turbulent spectra, no quantitative knowledge is available for predicting the effectiveness of active feedback control.

Very recently, we tried to theoretically investigate the Reynolds number effect on the drag reduction rate achieved by an idealized near-wall layer manipulation (Iwamoto et al., 2005). We assume that all velocity fluctuations in the near-wall layer, i.e., $0 < y < y_d$, are perfectly damped. We also assume a fully developed turbulent channel flow under a constant flow rate, and derived a theoretical relationship among the Reynolds number of the uncontrolled flow Re_τ , the dimensionless damping layer thickness y_d/δ , and the drag reduction rate R_D . It is given as:

$$\begin{aligned} \frac{1}{\kappa} \ln Re_\tau + F = \frac{y_d}{\delta} \left(1 - \frac{y_d}{\delta} + \frac{1}{3} \frac{y_d^2}{\delta^2} \right) (1 - R_D) Re_\tau \\ + \left(1 - \frac{y_d}{\delta} \right)^{\frac{3}{2}} (1 - R_D)^{\frac{1}{2}} \left[\frac{1}{\kappa} \ln \left\{ \left(1 - \frac{y_d}{\delta} \right)^{\frac{3}{2}} (1 - R_D)^{\frac{1}{2}} Re_\tau \right\} + F \right]. \end{aligned} \quad (18)$$

The sole empirical formula used in the derivation above is the Dean's formula (1978) on the bulk mean velocity (the logarithmic law version), i.e.,

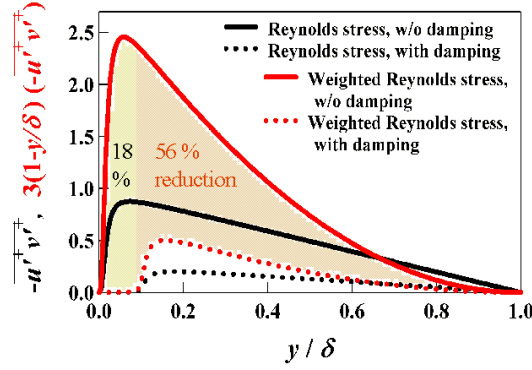


Figure 21 Reynolds shear stress in a channel flow at $Re_\tau = 650$ with idealized near-wall manipulation (Iwamoto et al., 2005).

$$\frac{U_b}{u_\tau} = \frac{1}{\kappa} \ln Re_\tau + F. \quad (19)$$

Figure 20(a) shows the dependency of R_D on Re_τ for constant values of y_d . As Re_τ increases, R_D decreases. The Reynolds number dependency of R_D , however, is found to be very mild. For $y_d^+ = 10$, for instance, the drag reduction rate R_D is about 43% at $Re_\tau = 10^3$, and about 35% even at $Re_\tau = 10^5$. The damping layer in the latter case is extremely thin as compared to the channel half width, i.e., $y_d/\delta = 0.01\%$.

The Reynolds number dependency of y_d required to achieve the same drag reduction rate R_D is shown in Fig. 20(b). As Re_τ increases, y_d gradually increases. For high Reynolds numbers, where $y_d/\delta \ll 1$ holds, Eq. (18) can reduce to $y_d^+ \sim \ln Re_\tau$, and this means the Reynolds number dependency is very weak. The asymptotic relation is in good agreement with Eq. (18) when $Re_\tau > 4 \times 10^3$ as shown in Fig. 24(b). Thus, large drag reduction can be obtained even at high Reynolds numbers if we can control and completely damp out the near-wall velocity fluctuations.

Figure 21 shows the Reynolds shear stress computed in the corresponding DNS. The friction Reynolds number is about 650 and the damped layer thickness is $y_d^+ = 60$. The Reynolds shear stress is drastically suppressed in the damping layer, and also decreased in the undamped region. The change in the Reynolds shear stress gives a clue to explain the large drag reduction through the FIK identity. As shown in Fig. 21, the drag reduction rate directly caused by the decrease of the Reynolds shear stress in the damped layer is 18%, while that due to the accompanied decrease of the Reynolds shear stress in the undamped region is 56%. For higher Reynolds numbers, the relative thickness of the damping layer y_d/δ becomes negligibly small, so that the contribution away from the damped layers should be dominant. Thus, possible large drag reduction at high Reynolds numbers should be mainly attributed to the decrease of the Reynolds stress in the region away from the wall.

The present theoretical analysis suggests the basic strategy behind the existing control schemes, i.e., attenuation of turbulence only in the near-wall layer, is also valid at high Reynolds numbers appearing in real applications.

6 Concluding Remarks

We introduced some major scientific and engineering accomplishments made in our five-year project “Smart Control of Turbulence: A Millennium Challenge for Innovative Thermal and Fluids Systems”. They are summarized as follows.

First, direct numerical simulation of active feedback control was carried out by assuming distributed sensors and actuators. A methodology based on the generic-algorithm was also developed to construct a practical control law. Based on these results, a prototype of the feedback control system for wall turbulence was developed with arrayed micro hot-film sensors and arrayed magnetic wall-deformation actuators. We have obtained about 7% skin friction reduction in a turbulent channel flow for the first time.

Direct numerical simulation of turbulent channel flow at $Re_\tau = 650$ and 1160 was made in order to examine the

dynamical roles of the large-scale outer-layer structures, and their relationship between the near-wall vortices. The streaky structures, of which spanwise spacing is about 100 wall units, exist only near the wall ($y^+ < 30$), while the large-scale structures exist from the center of the channel to the near-wall region. The energy transfer from the mean flow to the large-scale structures is indispensable for sustaining the large-scale structures. The quasi-streamwise vortices are located between low- and high-speed streaky structures in the near-wall region. Away from the wall, these small-scale vortices are clustered mostly in the low-speed large-scale structures. They agglomerate because of the advective motion of the large-scale structures.

We derived an identity equation that gives clear decomposition of different contributions to the skin friction, i.e., the FIK identity. Usefulness of the FIK identity was demonstrated through example analyses of drag reducing flows. For drag reduction control, suppression of the Reynolds stress near the wall is of primary importance. Based on this knowledge, an alternative cost functional, which incorporates the near-wall Reynolds shear stress distribution, was proposed in the framework of the suboptimal control.

We also derived a formula to describe the relationship between the Reynolds number and the drag reduction rate in turbulent channel flows by assuming an ideal damping of the velocity fluctuations in the near-wall layer. The derived formula indicates that large drag reduction can be attained even at high Reynolds numbers by suppressing the turbulence only near the wall, viz., without any direct manipulation of large-scale structures away from the wall. Therefore, the basic strategy behind the existing control schemes, i.e., attenuation of the near-wall turbulence only, is also valid at very high Reynolds numbers appearing in real applications.

Finally, despite the significant progress introduced here (and, of course, that made by other research groups), many issues still remain to be resolved before future real applications. For the hardware equipment, further downsizing of sensors/actuators, and development of actuators with low power consumption are required. In the software aspect, invention of groundbreaking control algorithms, which can much effectively reduce the near-wall Reynolds shear stress, is essential.

Acknowledgments

We thank former students at the University of Tokyo, who have been involved in this project, particularly, Drs. K. Iwamoto and T. Yoshino, for their creative and fine jobs. We are also grateful to Messrs. S. Kamiunten and N. Zushi at Yamatake Corp. for their help in manufacturing micro shear stress sensors.

This work was supported through the Project for Organized Research Combination System by the Ministry of Education, Culture, Sports and Technology of Japan (MEXT). The computer time for the present DNS at $Re_\tau = 1160$ was provided by the Earth Simulator Center, Japan.

References

- Adrian, R. J., Meinhart, C. D., and Tomkins, C. D., "Vortex organization in the outer region of the turbulent boundary layer," *J. Fluid Mech.*, Vol. 422, 2000, pp. 1-54.
- Bewley, T. R., "Flow control: new challenges for a new Renaissance," *Prog. Aerospace Sci.*, Vol. 37, 2001, pp. 21-58.
- Bewley, T. R., Moin, P., and Temam, R., "DNS-based predictive control of turbulence: an optimal benchmark for feedback algorithms," *J. Fluid Mech.*, Vol. 447, 2001, pp. 179-225.
- Choi, H., Moin, P., and Kim, J., "Active turbulence control for drag reduction in wall-bounded flows," *J. Fluid Mech.*, Vol. 262, 1994, pp. 75-110.
- Endo, T., Kasagi, N., and Suzuki, Y., "Feedback control of wall turbulence with wall deformation," *Int. J. Heat Fluid Flow*, Vol. 21, 2000, pp. 568-575.
- Fukagata, K., Iwamoto, K., and Kasagi, N., "Contribution of Reynolds stress distribution to the skin friction in wall-bounded flows," *Phys. Fluids*, Vol. 14, 2002, pp. L73-L76.
- Fukagata, K. and Kasagi, N., "Highly energy-conservative finite difference method for the cylindrical coordinate system," *J. Comput. Phys.*, Vol. 181, 2002, pp. 478-498.
- Fukagata, K. and Kasagi, N., "Drag reduction in turbulent pipe flow with feedback control applied partially to wall," *Int. J. Heat Fluid Flow*, Vol. 24, 2003, pp. 480-490.
- Fukagata, K. and Kasagi, N., "Suboptimal control for drag reduction via suppression of near-wall Reynolds shear stress," *Int. J. Heat Fluid Flow*, Vol. 25, 2004a, pp. 341-350.
- Fukagata, K. and Kasagi, N., "Feedback control of near-wall Reynolds shear stress in wall-turbulence," *Proc. 4th Int. Symp. Advanced Fluid Information and Transdisciplinary Fluid Integration*, Sendai, Nov. 2004, 2004b, pp.

346-351.

Fukagata, K., Kasagi, N., and Sugiyama, K., "Feedback control achieving sublamina friction drag," Proc. 6th Symp. Smart Control of Turbulence, Tokyo, March 2005 (downloadable from <http://www.turbulence-control.gr.jp/>), 2005.

Gad-el-Hak M., "Modern developments in flow control," Appl. Mech. Rev., Vol. 49, 1996, pp. 365-379.

Hamilton, J. M., Kim, J., and Waleffe, F., "Regeneration mechanisms of near-wall turbulence structures," J. Fluid Mech., Vol. 287, 1995, pp. 317-348.

Ho, C.-M. and Tai, Y.-C., "Review: MEMS and its applications for flow control," Trans. ASME J. Fluids Eng., Vol. 118, 1996, pp. 437-447.

Hou, Y. X., Somandepalli, V. S. R., and Mungal, M. G., "A technique to determine total shear stress and polymer stress profiles in drag reduced boundary layer flows," Exp. Fluids, Vol. 40, 2006, pp. 589-600.

Howarth, L., "On the solution of the laminar boundary layer equations," Proc. Roy. Soc. London Ser. A, Vol. 164, 1938, pp. 547-579.

Iwamoto K., Fukagata, K., Kasagi, N., and Suzuki Y., "Friction drag reduction achievable by near-wall turbulence manipulation at high Reynolds number," Phys. Fluids, Vol. 17, 2005, Art. 011702.

Iwamoto, K., Kasagi, N., and Suzuki, Y., "Dynamical Roles of Large-Scale Structures in Turbulent Channel Flow," Computational Mechanics, WCCM VI in conjunction with APCOM'04, Sept. 5-10, 2004, Beijing, China, MS022-174.

Iwamoto, K., Suzuki, Y., and Kasagi, N., "Reynolds number effect on wall turbulence: toward effective feedback control," Int. J. Heat Fluid Flow, Vol. 23, 2002, pp. 678-689.

Kasagi, N., "Progress in direct numerical simulation of turbulent transport and its control," Int. J. Heat Fluid Flow, Vol. 19, 1998, pp. 125-134.

Kasagi, N., Sumitani, Y., Suzuki, Y., and Iida, O., "Kinematics of the quasi-coherent vortical structure in near-wall turbulence," Int. J. Heat Fluid Flow, Vol. 16, 1995, pp. 2-10.

Kasagi, N., Suzuki, Y., and Fukagata, K., "Control of turbulence," Parity, Vol. 18, No. 2, 2003, pp. 20-26 (in Japanese) .

Kasagi, N., Kawaguchi, Y., Yoshida, H., Kodama, Y., and Ogawa, S., "Progress in smart control of turbulence," Proc. 6th Symp. Smart Control of Turbulence, March 2005, Tokyo, pp. 1-16. (URL: <http://www.turbulence-control.gr.jp/>)

Kim, J., "Control of turbulent boundary layers," Phys. Fluids, Vol. 15, 2003, pp. 1093-1105.

Kim, J., Moin, P., and Moser, R., "Turbulence statistics in fully developed channel flow at low Reynolds number," J. Fluid Mech., Vol. 177, 1987, pp. 133-166.

Kline, S. J., Reynolds, W. C., Schraub, F. A., and Runstadler, P. W., "The structure of turbulent boundary layers," J. Fluid Mech., Vol. 30, 1967, pp. 741-773.

Koumoutsakos, P., "Vorticity flux control for a turbulent channel flow," Phys. Fluids, Vol. 11, 1998, pp. 248-250.

Kravchenko, A. G., Choi, H., and Moin, P., "On the relation of near-wall streamwise vortices to wall skin friction in turbulent boundary layers," Phys. Fluids A, Vol. 5, No. 12, 1993, pp. 3307-3309.

Lee, C., Kim, J., Babcock, D., and Goodman, R., "Application of neural networks to turbulence control for drag reduction," Phys. Fluids, Vol. 9, 1997, pp. 1740-1747.

Lee, C., Kim, J., and Choi, H., "Suboptimal control of turbulent channel flow for drag reduction," J. Fluid Mech., Vol. 358, 1998, pp. 245-258.

Lee, K. H., Cortelezzi, L., Kim, J., and Speyer, J., "Application of reduced-order controller to turbulent flows for drag reduction," Phys. Fluids, Vol. 13, 2001, pp. 1321-1330.

Li, F.-C., Kawaguchi, Y., and Hishida, K., "Investigation on the characteristics and turbulent transport for momentum and heat in a drag-reducing surfactant solution flow," Phys. Fluids, Vol. 16, 2004, pp. 3281-3295.

Moin, P., and Bewley, T., "Feedback control of turbulence," Appl. Mech. Rev., Vol. 47, 1994, pp. S3-S13.

Morimoto, K., Iwamoto, K., Suzuki, Y., and Kasagi, N., "Genetic algorithm-based optimization of feedback control scheme for wall turbulence," Proc. 3rd Symp. Smart Control of Turbulence, March 2002, Tokyo (downloadable from <http://www.turbulence-control.gr.jp/>), 2002, pp. 107-113.

Moser, R. D., Kim, J., and Mansour, N. N., "Direct numerical simulation of turbulent channel flow up to $Re_\tau = 590$," Phys. Fluids, Vol. 11, No. 4, 1999, pp. 943-945.

Robinson S. K., "Coherent motions in the turbulent boundary layer," Annu. Rev. Fluid Mech., Vol. 23, 1991, pp. 601-639.

Sumitani, Y., and Kasagi, N., "Direct numerical simulation of turbulent transport with uniform wall injection and suction," *AIAA J.*, Vol. 33, 1995, pp. 1220-1228.

Suzuki, Y., Yoshino, T., Yamagami, T., and Kasagi, N., "Drag Reduction in a Turbulent Channel Flow by Using a GA-based Feedback Control System," Proc. 6th Symp. Smart Control of Turbulence, Tokyo, March 2005, (downloadable from <http://www.turbulence-control.gr.jp/>), 2005.

Yamagami, T., Suzuki, Y., and Kasagi, N., "Development of feedback control system of wall turbulence using MEMS devices," Proc. 6th Symp. Smart Control of Turbulence, Tokyo, March 2005, (downloadable from <http://www.turbulence-control.gr.jp/>), 2005.

Yoshino, T., Suzuki, Y., and Kasagi, N., "Evaluation of GA-based feedback control system for drag reduction in wall turbulence," Proc. 3rd Int. Symp. Turbulence and Shear Flow Phenomena, Sendai, June 2003, 2003a, pp. 179-184.

Yoshino, T., Suzuki, Y., Kasagi, N., and Kamiunten, S., "Optimum Design of Micro Thermal Flow Sensor and Its Evaluation in Wall Shear Stress Measurement," Proc. 16th IEEE Int. Conf. MEMS2003, Kyoto, Jan. 2003, 2003b, pp. 193-196.

Yu, B., Li, F., and Kawaguchi, Y., "Numerical and experimental investigation of turbulent characteristics in a drag-reducing flow with surfactant additives," *Int. J. Heat Fluid Flow*, Vol. 25, 2004, pp. 961-974.

Zagarola, M. V. and Smits, A. J., "Mean-flow scaling of turbulent pipe flow," *J. Fluid Mech.*, Vol. 373, 1998, pp. 33-79.

Xu, C.-X., Choi, J.-I., and Sung H.J., "Suboptimal control for drag reduction in turbulent pipe flow," *Fluid Dyn. Res.*, Vol. 30, 2002, pp. 217-231.

Zhou, J., Adrian, R. J., Balachandar, S., and Kendall, T. M., "Mechanisms for generating coherent packets of hairpin vortices in channel flow," *J. Fluid Mech.*, Vol. 387, 1999, pp. 353-396.